Efficient synthesis of π-extended phenazasilines for optical and electronic applications

Huanhuan Li[a], Yang Wang[a], Kai Yuan[a], Ye Tao[a], Runfeng Chen[*a], Chao Zheng[a], Xinhui Zhou[a], Junfeng Li[a], Wei Huang[*a,b]

[a]Key Laboratory for Organic Electronics and Information Displays & Institute of Advanced Materials (IAM), National Synergistic Innovation Center for Advanced Materials (SICAM), Nanjing University of Posts and Telecommunications (NUPT), 9 Wenyuan Road, Nanjing, 210023, P.R. China.
E-mail: iamrfchen@njupt.edu.cn; wei-huang@njupt.edu.cn. Fax: +86 25 8586 6396. Tel: +86 25 8586 6396
[b]Key Laboratory of Flexible Electronics (KLOFE) & Institute of Advanced Materials (IAM), National Synergistic Innovation Center for Advanced Materials (SICAM), Nanjing Tech University (Nanjing Tech), 30 South Puzhu Road, Nanjing 211816, PR. China.

Table of Contents

1. Materials and Synthesis 2
2. Single crystal X-ray analysis 11
3. Thermal Properties 12
4. Atom force microscopy 13
5. Optical Properties 13
6. Electrochemical Properties 15
7. Theoretical calculations 15
8. Device fabrication and measurements 19
9. References 21

1. Materials and Synthesis

The chemicals and solvents, unless otherwise specified, were purchased from Aldrich, Acros, or Alfa Aesar, and used without further purification. The manipulations involving air-sensitive reagents were performed in an atmosphere of dry N_2. Tetrahydrofuran (THF) and 1,4-dioxane were dried and purified by routine procedures. ^{1}H and ^{13}C-nuclear magnetic resonance (NMR) spectra were recorded on a Bruker Ultra Shied Plus 400 MHz instrument with *d*-DMSO or *d*-$CDCl_3$ as the solvents and tetramethylsilane (TMS) as the internal standard. The quoted chemical shifts are in *ppm* and the *J* values are expressed in Hz. The splitting patterns have been designed as follows: s (singlet), d (doublet), t (triplet), dd (doublet of doublets), and m (multiplet).

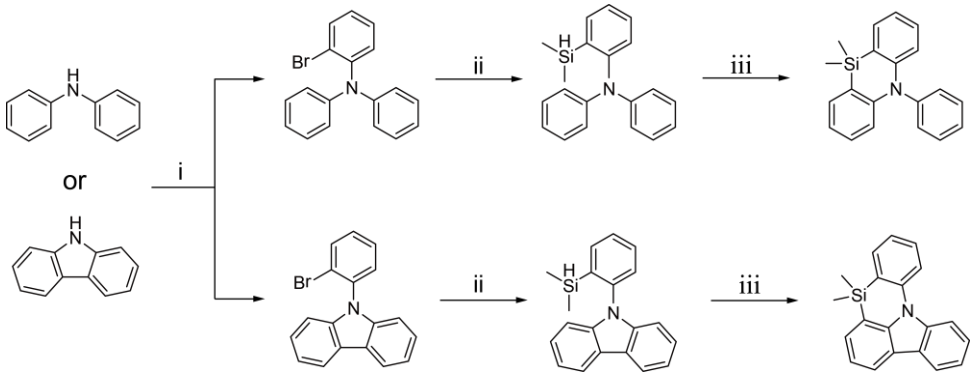

Scheme S1: The synthetic route of phenazasiline derivatives: (i) 2-bromoiodobenzene, Cu_2O, K_3PO_4, xylene, 120°C, 48 h; (ii) *n*-BuLi, chlorodimethylsilane, THF, -78°C to room temperature, 10 h; (iii) $RhCl(PPh_3)_3$, 3,3-dimethyl-1-butene, 1,4-dioxane, 135°C, 24 h.

The synthesis of 2-bromo-N,N-diphenylaniline

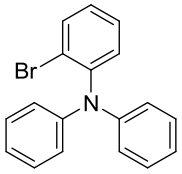

Diphenylamine (8.46 g, 50 mmol), 2-bromoiodobenzene (12.75 mL, 100 mmol), copper(I) oxide (1.43 g, 10 mmol), N,N'-dimethylethylenediamine (2.15 mL, 20 mmol) and anhydrous potassium phosphate (23.35 g, 110 mmol) were mixed and dissolved in xylene (40 mL). The mixture was then heated at 120°C for 2 days.[1] After the completion of the reaction, the mixture was poured into 1.0 M NH_4OH aqueous solution and extracted with dichloromethane (DCM) for three times (3×200 mL). The organic phase was separated, collected, dried, and concentrated under reduced pressure. The crude solid product was further purified by flash column chromatography on silica

gel (300-400 mesh). Yield: 9.3 g of white solid (55%). ^{1}H NMR (400 MHz, $CDCl_3$, ppm): δ 7.71 (d, J=8 Hz 1H), 7.44 (t, J=7.6 Hz 1H), 7.29-7.22 (m, 5H), 6.95 (t, J=7.4 Hz 1H), 6.83 (t, J=7.6 Hz 6H). ^{13}C NMR (100 MHz, $CDCl_3$, ppm) 146.98, 145.50, 134.54, 131.67, 129.06, 128.85, 127.29, 123.77, 122.03, 121.98.

The synthesis of 2-(dimethylsilyl)-N,N-diphenylaniline

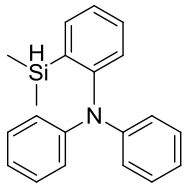

To a solution of 2-bromo-N,N-diphenylaniline (3.2 g, 10 mmol) in freshly distilled THF (50 mL) was added a hexane solution of *n*-BuLi (6.6 mL, 1.6 M, 10.5 mmol) dropwise at -78°C. After the reaction mixture was stirred for 1.5 h, chlorodimethylsilane (1.3 mL, 12 mmol) was added. The reaction was allowed to warm to room temperature and stirred overnight. The reaction was quenched with water (15 mL) and extracted with DCM (3×50 mL). The organic layers were collected and dried with anhydrous Na_2SO_4. The solvent was removed under reduced pressure. The crude product was purified by flash column chromatography on silica gel. Yield: 2.8 g of white solid (93%). ^{1}H NMR (400 MHz, *d*-DMSO, ppm): δ 7.83 (d, J=6 Hz 1H), 7.74 (t, J=7.6 Hz 1H), 7.56 (t, J=7.4 Hz 1H), 7.44 (d, J=7.6 Hz 1H), 7.06 (d, J=7.2 Hz 2H), 6.91-6.82 (m, 4H), 6.03 (d, J=8.0 Hz 2H), 4.29-4.25 (m, 1H), 0.07 (d, J=3.6 Hz 6H). ^{13}C NMR (100 MHz, *d*-DMSO, ppm) 150.17, 149.27, 143.37, 143.07, 137.54, 137.07, 133.72, 132.37, 131.82, 127.91, 124.11, 120.75, 1.25.

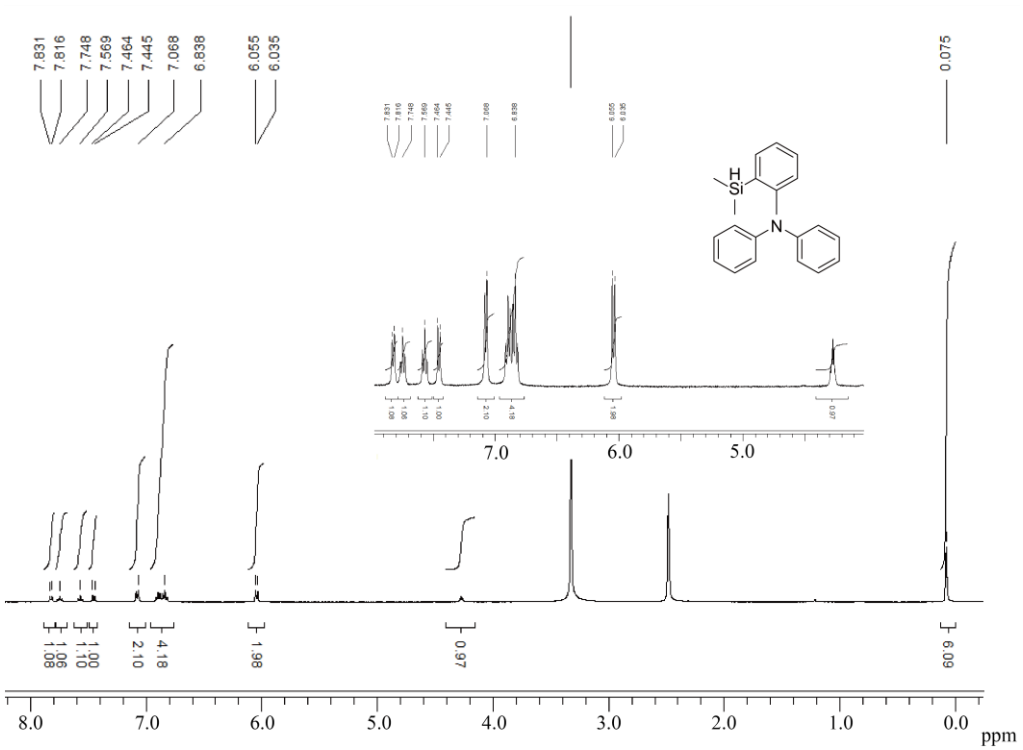

Figure S1. ^{1}H NMR spectrum of 2-(dimethylsilyl)-N,N-diphenylaniline

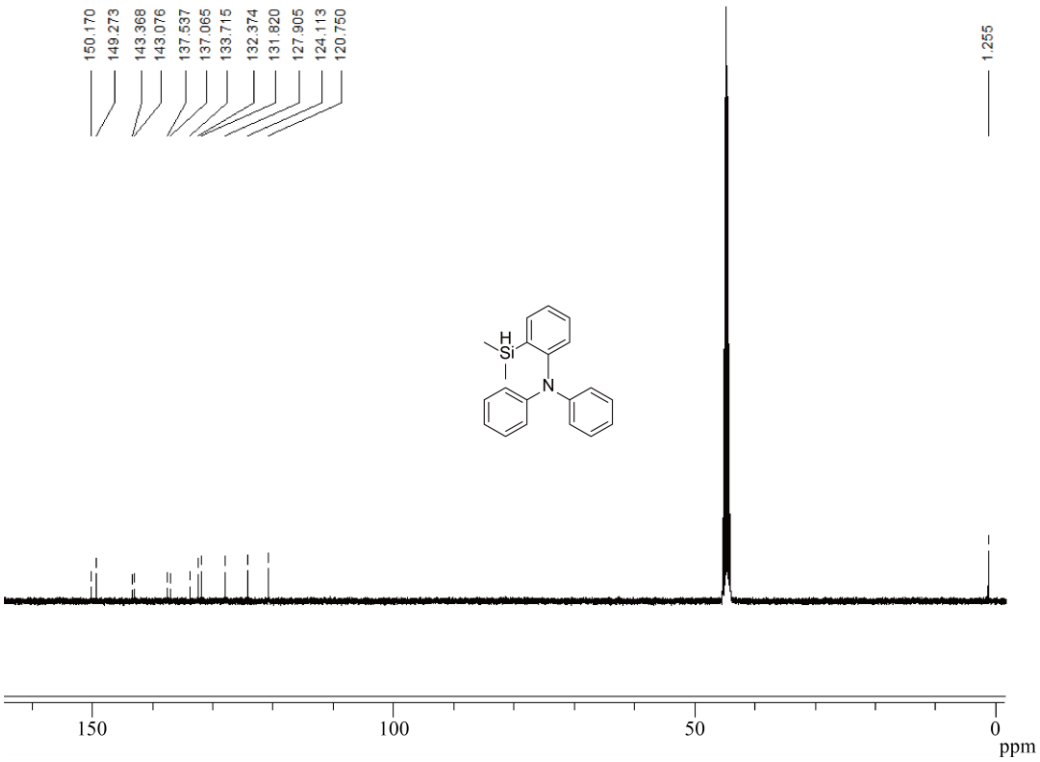

Figure S2. ^{13}C NMR spectrum of 2-(dimethylsilyl)-N,N-diphenylaniline

The synthesis of 10,10-dimethyl-5-phenyl-diphenylphenazasiline (TPASi)

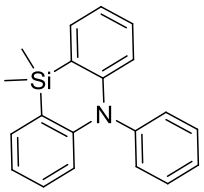

A mixture of 2-(dimethylsilyl)-N,N-diphenylaniline (0.15 g，0.5 mmol), 3,3-dimethyl-1-butene (0.32 mL, 2.5 mmol), $RhCl(PPh_3)_3$ (2.3 mg，0.0025 mmol), and 1,4-dioxane (5 mL) was stirred at 135℃ for 24 h. Then, the solvent was removed in vacuum and the product was isolated by column chromatography on silica gel to give 10,10-dimethyl-5-phenyl-5,10-diphenylphenazasiline. Yield: 0.13 g white solid (92%). ^{1}H NMR (400 MHz, $CDCl_3$, ppm): δ 7.62 (t, J=8 Hz 2H), 7.55 (dd, J=7.2 Hz 2H), 7.50 (t, J=7.6 Hz 1H), 7.29 (t, J=8.4 Hz 2H), 7.11 (t, J=8.0 Hz 2H), 6.94 (t, J=6.4 Hz 2H), 6.30 (d, J=7.2 Hz 2H), 0.51 (s, 6H). ^{13}C NMR (100 MHz, $CDCl_3$, ppm) 149.29, 143.76, 134.23, 131.27, 130.98, 129.82, 127.92, 119.62, 118.75, 116.88, 0.53.

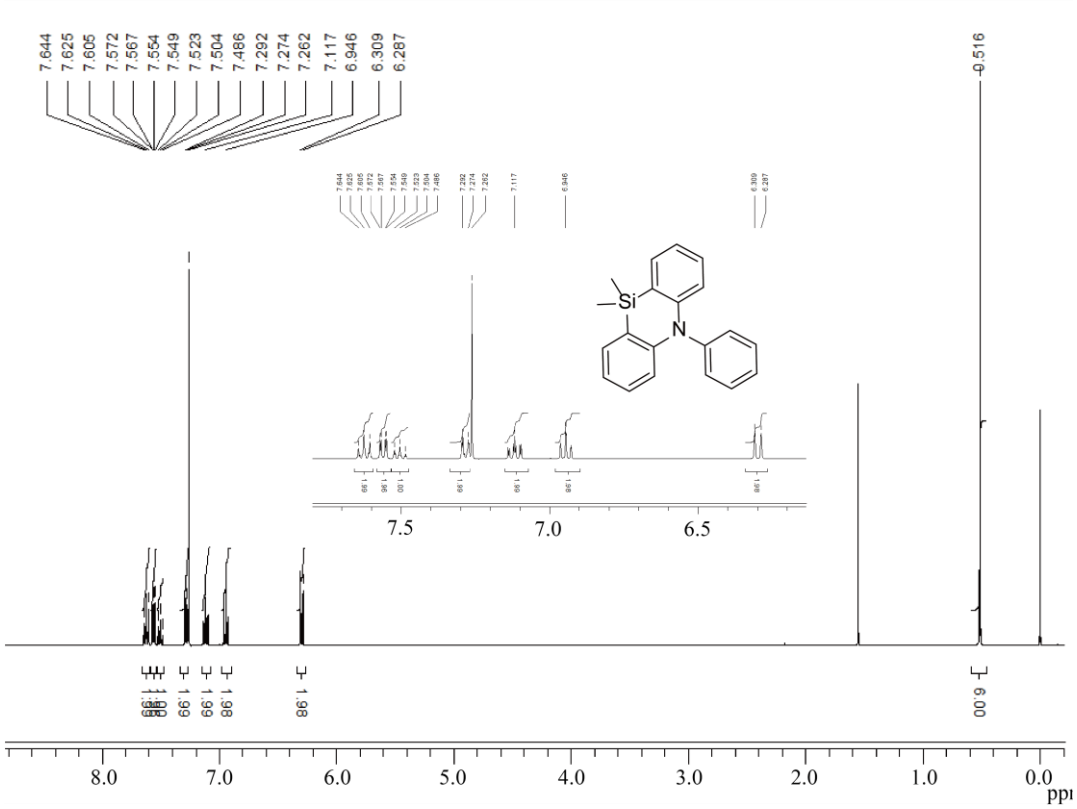

Figure S3. ^{1}H NMR spectrum of 10,10-dimethyl-5-phenyl-diphenylphenazasiline

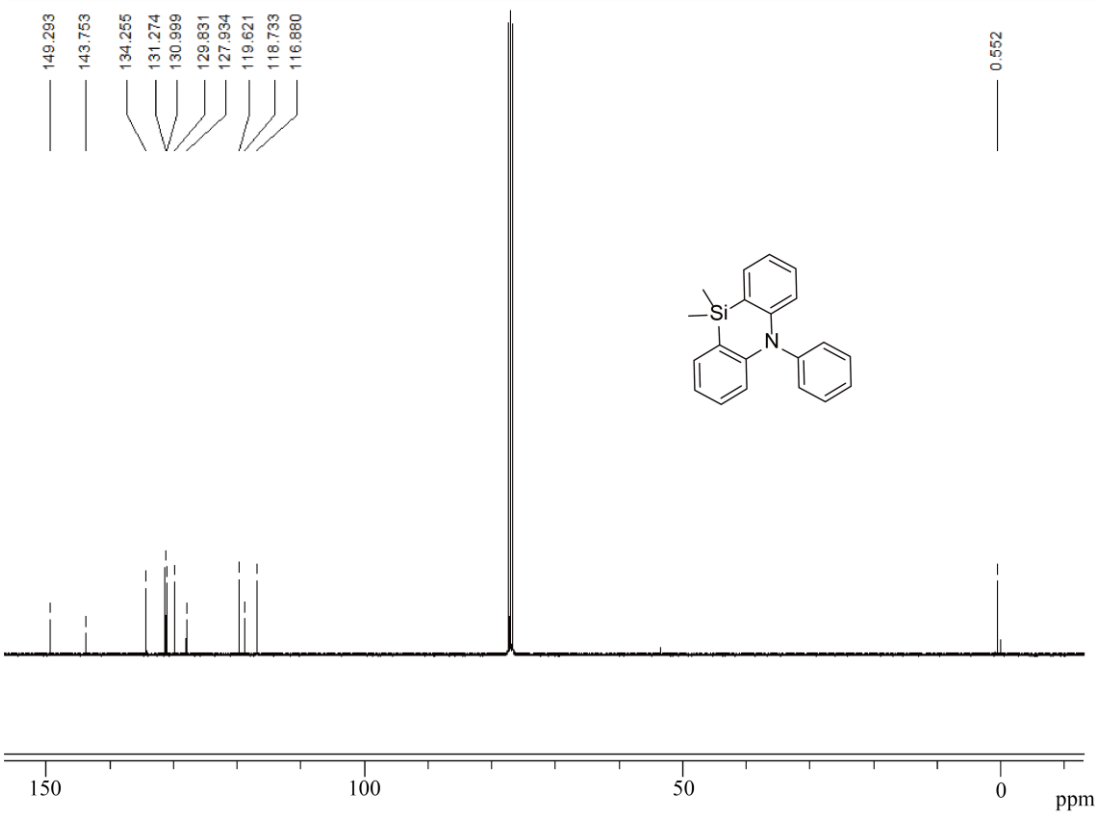

Figure S4. ^{13}C NMR spectrum of 10,10-dimethyl-5-phenyl-diphenylphenazasiline

The synthesis of 9-(2-bromophenyl)-9H-carbazole

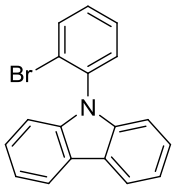

The 9-(2-bromophenyl)-9H-carbazole was prepared in an identical synthetic procedure of 2-bromo-N,N-diphenylaniline using carbazole, 2-bromoiodobenzene, copper(I) oxide, N,N'-dimethylethylenediamine and anhydrous potassium phosphate in xylene. Yield: 65% white solid. ^{1}H NMR (400 MHz, $CDCl_3$, ppm): δ 7.08 (m, 2H), 7.35-7.56 (m, 7H), 7.91 (d, J = 8.0 Hz, 1H), 8.17 (d, J = 7.6 Hz, 2H); ^{13}C NMR (100 MHz, $CDCl_3$, ppm) 114.29, 116.72, 117.87, 120.68, 120.85, 121.09, 121.74, 122.68, 122.89, 124.98, 125.99, 126.01, 130.08, 135.20, 139.33, 144.25, 144.56.

The synthesis of 9-(2-(dimethylsilyl)phenyl)-9H-carbazole

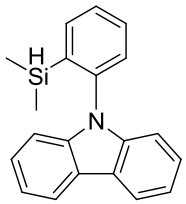

The 9-(2-(dimethylsilyl)phenyl)-9H-carbazole was prepared in an identical synthetic procedure of 2-(dimethylsilyl)-N,N-diphenylaniline. Yield: 90% white solid. ^{1}H NMR (400 MHz, *d*-DMSO, ppm): δ 8.20 (d, J=7.6 Hz 2H), 7.83 (t, J=7.2 Hz 1H), 7.70-7.61 (m, 2H), 7.38-7.31 (m, 3H), 7.23 (t, J=7.4 Hz 2H), 6.92 (d, J=8.0 Hz 2H), 3.74-3.71 (m, 1H), -0.18 (d, J=3.6 Hz 6H). ^{13}C NMR (100 MHz, *d*-DMSO, ppm) 142.28, 142.17, 138.15, 136.93, 132.27, 129.66, 129.22, 126.46, 122.67, 120.88, 120.05, 110.36, -3.56.

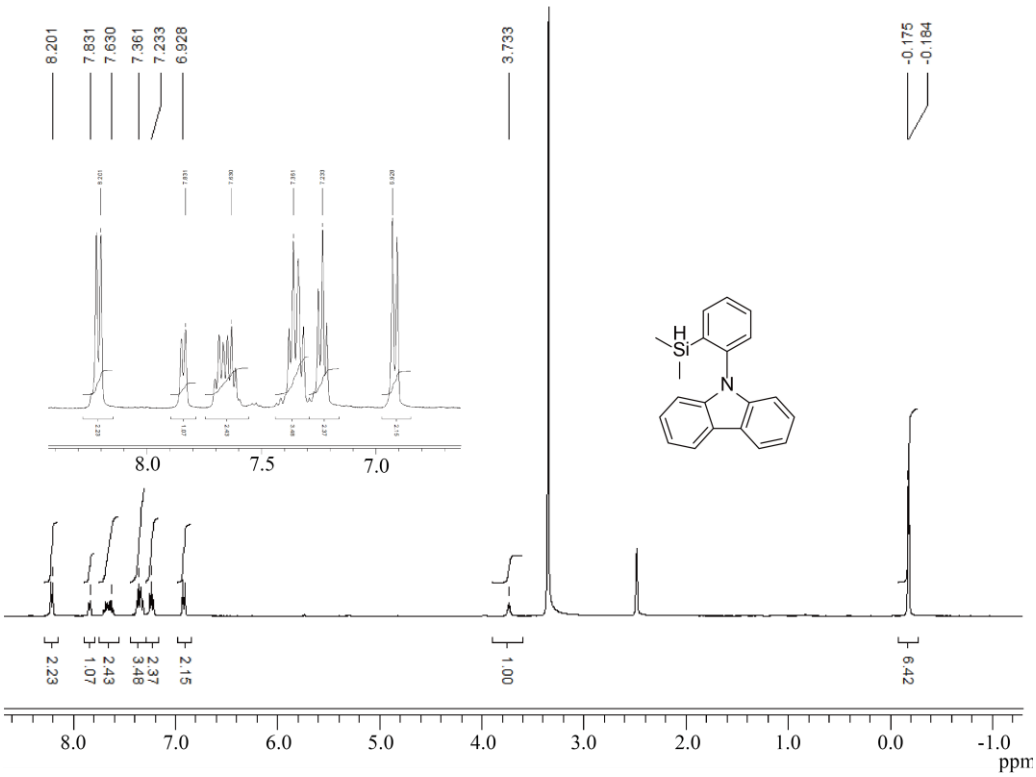

Figure S5. ^{1}H NMR spectrum of 9-(2-(dimethylsilyl)phenyl)-9H-carbazole

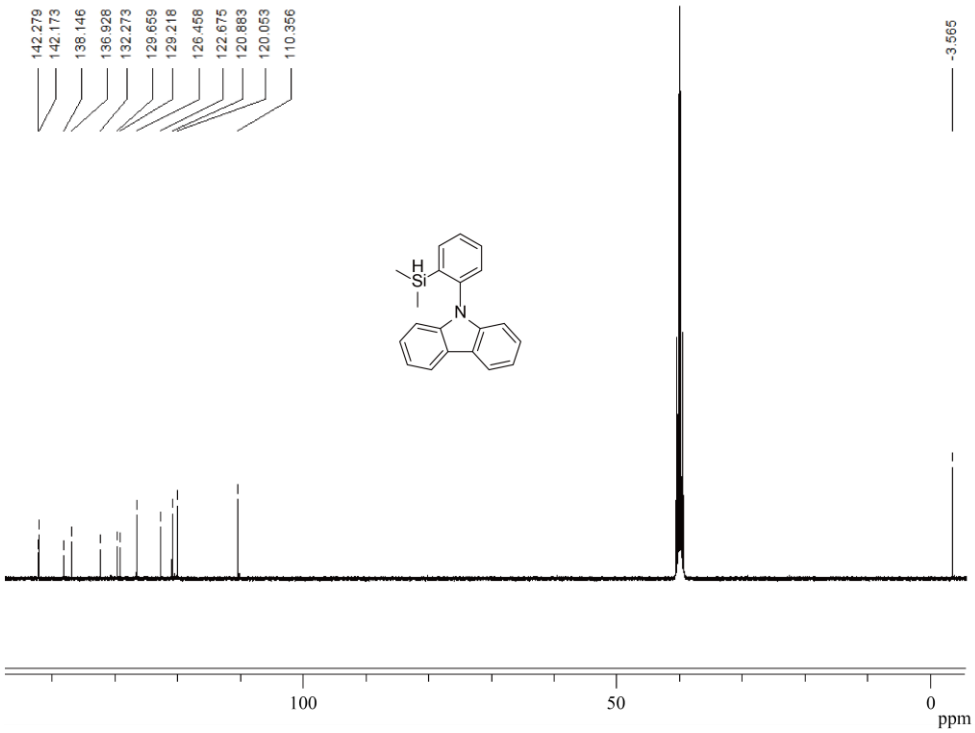

Figure S6. ^{13}C NMR spectrum of 9-(2-(dimethylsilyl)phenyl)-9H-carbazole

The synthesis of 5,5-dimethyl-5H-benzo[5,6][1,4]azasilino[3,2,1-jk]carbazole (PhCzSi)

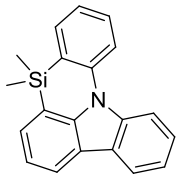

The 5,5-dimethyl-5H-benzo[5,6][1,4]azasilino[3,2,1-jk]carbazole (PhCzSi) was prepared in the same procedure of 10,10-dimethyl-5-phenyl-diphenylphenazasiline. Yield: 92% white solid. ^{1}H NMR (400 MHz, $CDCl_3$, ppm): δ 8.21 (d, J=8.4 Hz 2H), 8.12 (t, J=6.4 Hz 2H), 7.73 (dd, J=9.6 Hz 1.6 Hz 1H), 7.68 (dd, J=9.6 Hz 1.6 Hz 1H), 7.50 (t, J=8.0 Hz 2H), 7.41 (t, J=6.4 Hz 1H), 7.33 (t, J=8.4 Hz 1H), 7.22 (d, J=7.2 Hz 1H), 0.52 (s, 6H). ^{13}C NMR (100 MHz, $CDCl_3$, ppm) 144.56, 144.25, 139.33, 135.21, 130.80, 130.09, 126.01, 124.99, 122.90, 122.70, 121.74, 121.09, 120.86, 120.68, 117.87, 116.72, 114.29, -0.40.

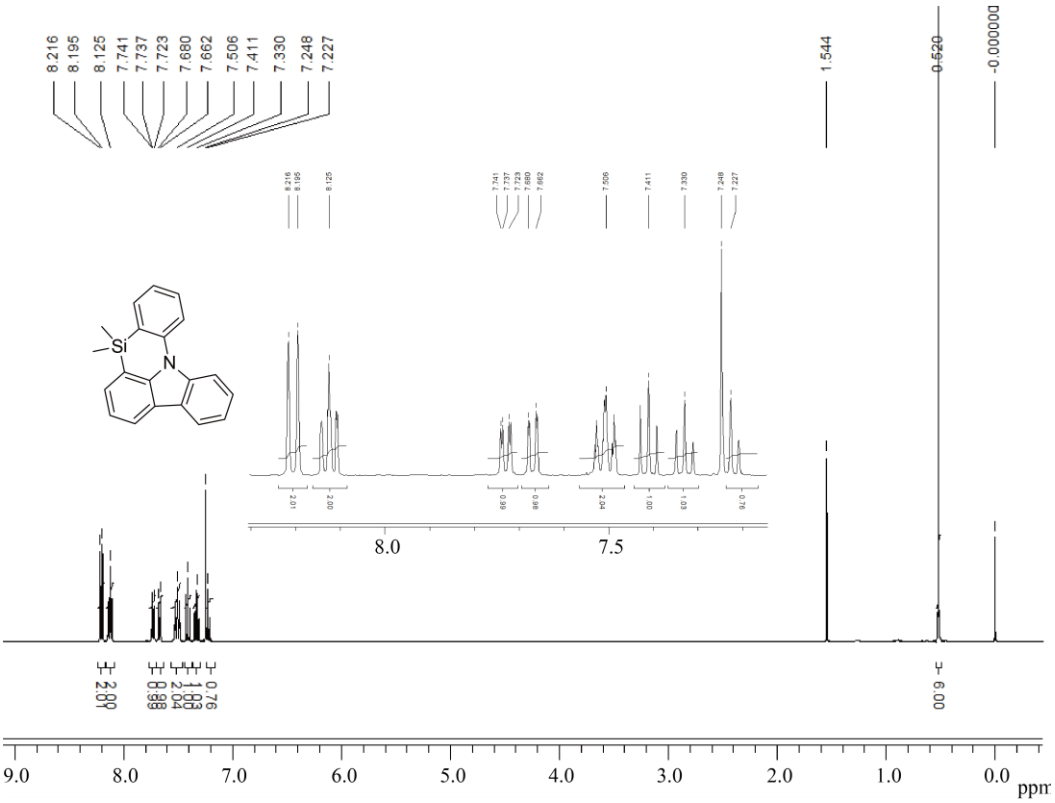

Figure S7. ^{1}H NMR spectrum of 5,5-dimethyl-5H-benzo[5,6][1,4]azasilino[3,2,1-jk]carbazole

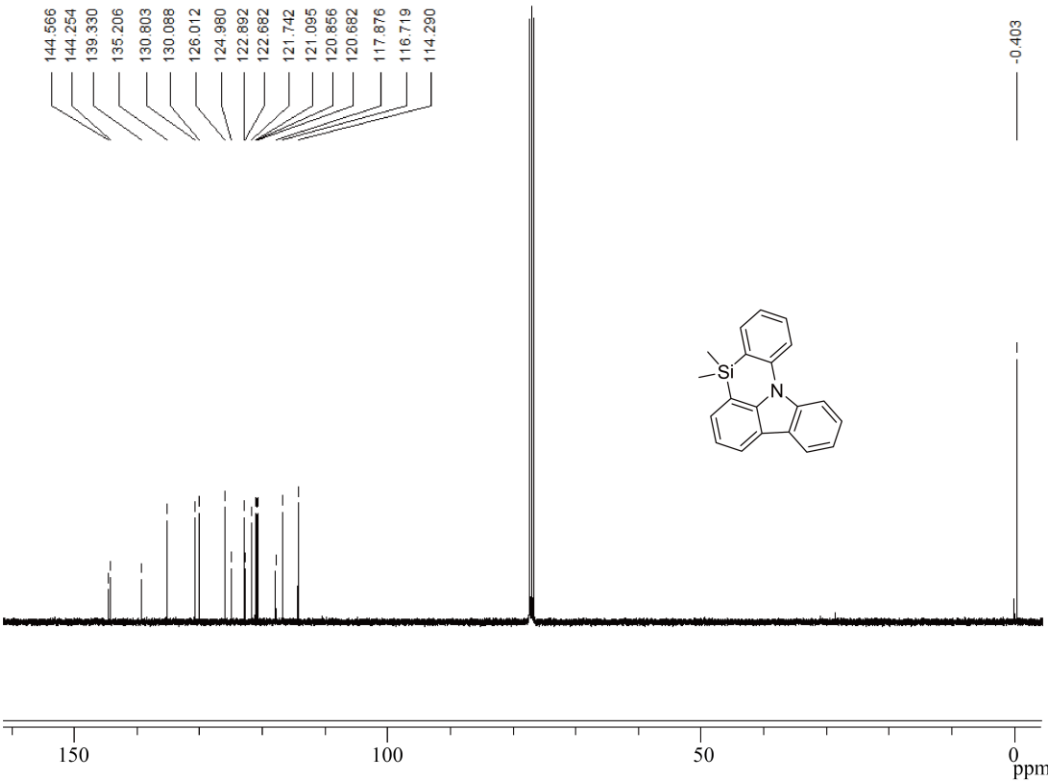

Figure S8. ^{13}C NMR spectrum of 5,5-dimethyl-5H-benzo[5,6][1,4]azasilino[3,2,1-jk]carbazole

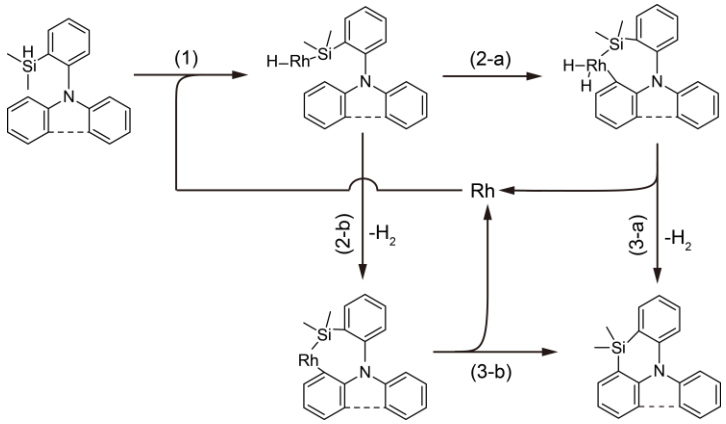

Scheme S2: Proposed mechanism for Rhodium-catalyzed synthesis of phenazasiline derivatives.

The possible mechanism for this novel synthesis of phenazasilines from diarylhydrosilanes was depicted in **Scheme S2**. According to the previously reported rhodium-catalyzed cleavage of Si-H and C-H bonds in the preparation of five-membered silafluorene[2], the formation of six-membered phenazasiline may also involve the following three steps: (1) oxidative addition of the hydrosilane to a metal center (Si-H bond activation); (2-a) sequential oxidative addition of the aromatic C-H bond to the metal center (C-H bond activation); (3-a) reductive elimination to give the phenazasilines. Alternatively, another possible pathway is: (2-b) the formation of the intermediate via σ-bond metathesis (C-H bond activation); (3-b) reductive elimination via dehydrogenation to give phenazasilines. The high cyclization efficiency in the formation of phenazasilines may be because Si-Rh-H moiety is close to the C-H bond for easy intramolecular Si-H and C-H cleavages in step (2-a) or (2-b).

2. Single crystal X-ray analysis

Single crystals of the phenazasiline derivatives were grown by slow evaporation of a combined DCM and ethanol solution at room temperature. The single crystal structure data were collected on a Bruker SMART APEX (II)-CCD at 296 K and were analyzed by Mercury 1.4 software. Their structure data were summarized in Table S1. The crystallographic information file (CIF) files of the two single crystals of TPASi and PhCzSi were also attached.

Table S1. Crystallographic Data of TPASi and PhCzSi

Compound	**TPASi**	**PhCzSi**
Empirical formula	$C_{20}H_{19}NSi$	$C_{20}H_{17}NSi$
Formula weight g mol^{-1}	301.45	299.44
Crystal color	colorless	colorless
Wavelength Å	0.71073	0.71073
Crystal system	monoclinic	monoclinic
a, Å	11.649(4)	9.4672(19)
b, Å	8.213(3)	17.673(4)
c, Å	17.429(6)	10.494(2)
α, °	90	90
β, °	93.953(4)	115.360(2)
γ, °	90	90
volume, Å^3	1663.6(9)	1586.6(6)
Z	4	4
Density, g cm^{-3}	1.204	1.254
μ, mm^{-1}	0.137	0.144
Tmin, Tmax	0.981,0.984	0.980,0.983
F(000)	640.0	632.0
hmax, kmax, lmax	12,8,17	11,21,12
Theta$_{max}$	21.570	25.000

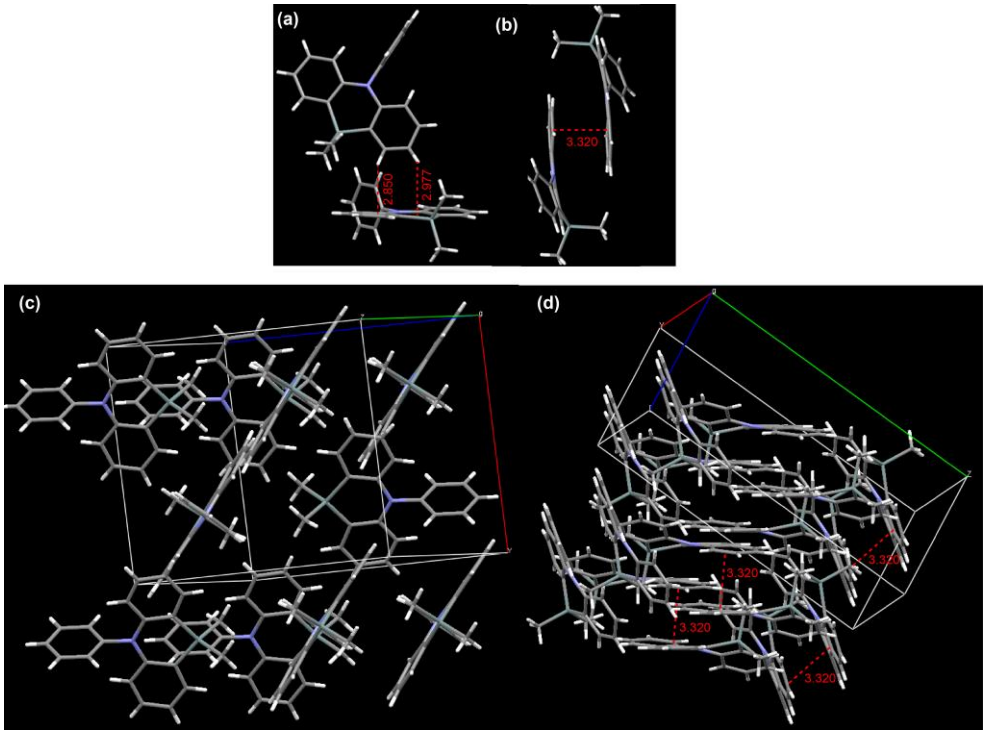

Figure S9. Molecular packing structures of TPASi (a, c) and PhCzSi (b, d) in dimer (a, b) and crystal (c, d) revealed by X-ray crystallographic analysis.

3. Thermal Properties

Thermogravimetric analyses (TGA) were conducted on a Shimadzu DTG-60H thermogravimetric analyses under a heating rate of 10°C/min and a nitrogen flow rate of 50 cm^3/min. Differential scanning calorimetry (DSC) analyses were performed on a Shimadzu DSC-60A instrument with a heating rate of 10°C/min and an nitrogen flow rate of 20 cm^3/min.

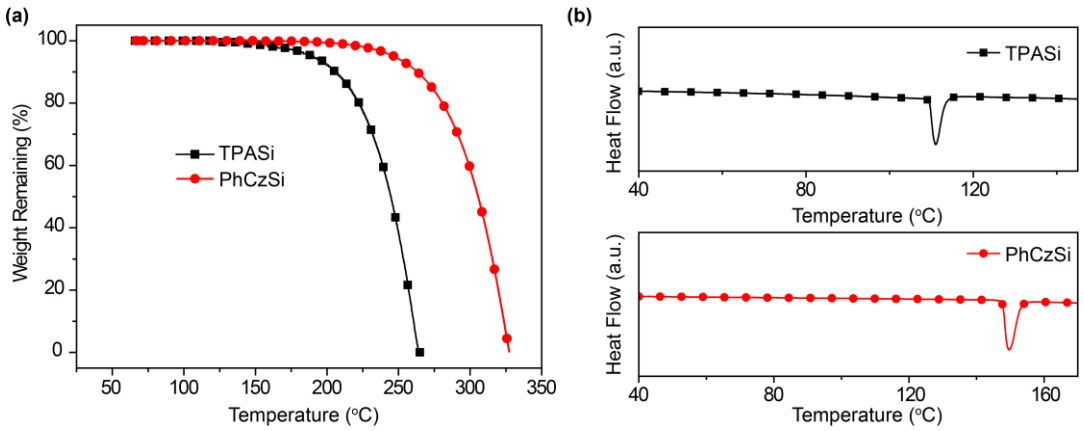

Figure S10. The (a) TGA and (b) DSC curves of TPASi and PhCzSi.

4. Atom force microscopy

To investigate the surface image and amorphous stability of the PhCzSi thin film, atomic force microscopy (AFM) was carried out at room temperature using a Bruker Dimension Icon AFM equipped with Scanasyst-Air peak force tapping mode AFM tips from Bruker. The surface height images of PhCzSi thin film (50 nm) vacuum-deposited on ITO surface were examined before and after thermal annealing at 100°C for 30 min; the scan size is 5×5 μm^2.

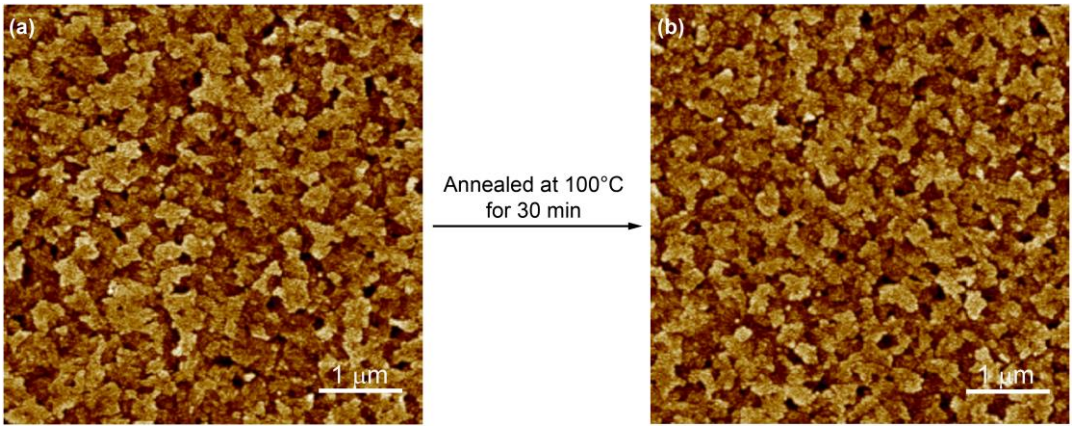

Figure S11. The AFM height images (5×5 μm^2) of the PhCzSi thin film (50 nm) vacuum-deposited on ITO surface: (a) as-prepared, (b) annealed at 100ºC for 30 min.

5. Optical Properties

Ultraviolet/visible (UV/Vis) spectra were recorded on an SHIMADZU UV-3600 UV/Vis-NIR spectrophotometer, while fluorescence spectra were obtained using an RF-5301PC spectrofluorophotometer with a Xenon lamp as light source. The photoluminescence quantum yield (PLQY) of the compounds (in DCM, 1.3×10^{-6} mol L^{-1}) were measured using an Edinburgh FLSP920 fluorescence spectrophotometer equipped with a xenon arc lamp (Xe900) using an integrating sphere. The phosphorescence spectra of the compounds (in DCM) were measured using an Edinburgh LFS920 fluorescence spectrophotometer at 77 K, with a 5 ms delay time after excitation with a microsecond flash lamp. The drop-cast films were prepared by casting solutions of the compounds on quartz substrates. The solvent effects on the absorption and emission of these phenazasiline derivatives were investigated by orientational polarizability (Δf), which was chosen as the measure of the solvent polarity and calculated using Equation 1[3]:

$$\Delta f = \frac{\varepsilon - 1}{2\varepsilon + 1} - \frac{n^2 - 1}{2n^2 + 1} \quad \ldots\ldots\ldots\ldots\ldots\ldots\ldots\ldots\ldots\ldots 1$$

where ε is the static dielectric constant and n is the optical refractive index of the solvent.

Table S2. Steady-state absorption (λ_a) and emission (λ_f) peaks in different solvents with varied polarity, dielectric constant (ε), and refractive index (n).

solvent	polarity	ε	n	Δf	TPA		TPASi		PhCz		PhCzSi	
					λ_a	λ_f	λ_a	λ_f	λ_a	λ_f	λ_a	λ_f
Cyclohexane	0.1	2.00	1.427	0.003	300	354	288	338	293	347	299	366
DCM	3.4	9.1	1.424	0.218	301	363	291	345	293	353	298	374
THF	4.2	7.58	1.405	0.210	300	365	289	347	293	351	298	371
Ethanol	4.3	24.5	1.3	0.312	299	358	288	341	292	350	297	365
Ethyl Acetate	4.3	6.02	1.370	0.201	298	356	288	342	292	350	297	370
Acetonitrile	6.2	35.94	1.341	0.306	297	360	287	348	291	352	296	375

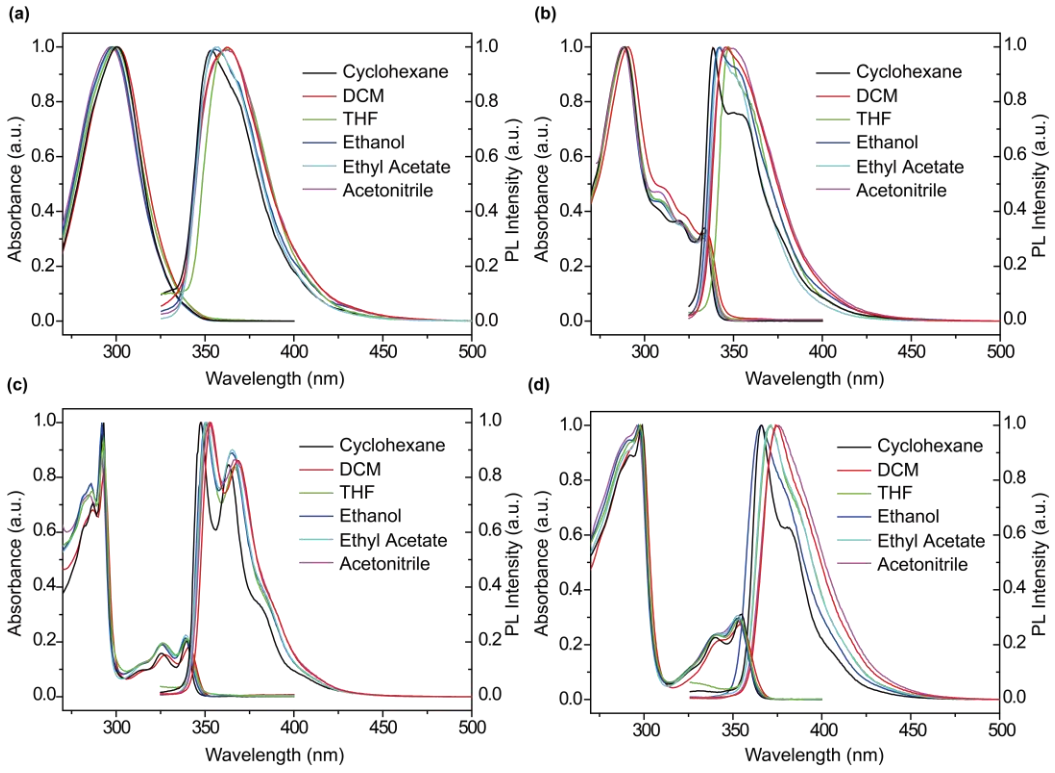

Figure S12. Normalized optical absorption and PL spectra of (a) TPA (b) TPASi (c) PhCz and (d) PhCzSi in different solvents.

6. Electrochemical Properties

The highest occupied molecular orbital (HOMO), the lowest unoccupied molecular orbital (LUMO), and the energy gap between them (E_g) can be measured by cyclic voltammetry (CV). The CV measurements were performed at room temperature on a CHI660E system in a typical three-electrode cell with a working electrode (glass carbon), a reference electrode (Ag/Ag^+, referenced against ferrocene/ferrocenium (FOC)), and a counter electrode (Pt wire) in an acetonitrile solution of tetrabutylammonium hexafluorophosphate (Bu_4NPF_6) (0.1 M) at a sweeping rate of 100 mVs^{-1}. The HOMO energy levels can be estimated based on the reference energy level of ferrocene (-4.8 eV): E_{HOMO}= -[E_{onset}-(0.04)+4.8], where the value of 0.04 V is the onset oxidative voltage of FOC *vs* Ag/Ag^+ and E_{onset} is the oxidative onset voltage of the measured compounds.

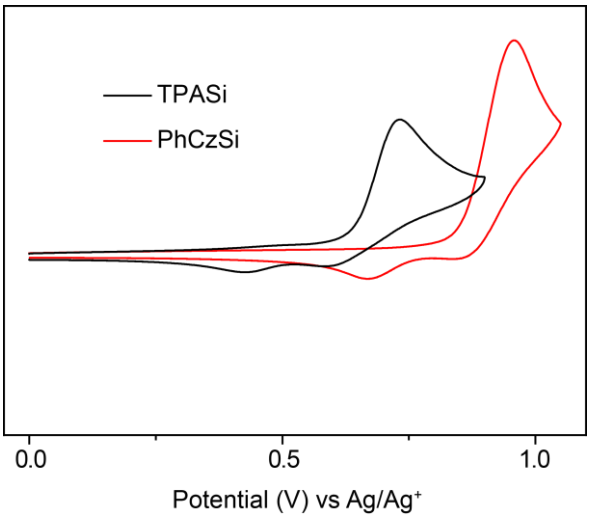

Figure S13. Cyclic voltammograms of TPASi (black) and PhCzSi (red) thin solid films.

7. Theoretical calculations

The density functional theory (DFT) computations were carried out with Gaussion 09 program package for structure optimizations and vibrational analyses. The ground-state (S_0) and the lowest triplet excited state (T_1) geometries were fully optimized by the Becker's three-parameter exchange functional along with the Lee Yang Parr's correlation functional (B3LYP) using 6-31G (d) basis sets; the lowest singlet excited-state (S_1) geometries were optimized by using the time-dependent density functional theory (TD-DFT) method with the same basis set.[4] These fully optimized stationary points were further characterized by harmonic

vibrational frequency analysis to ensure that real local minima were found. The lowest triplet state energy was evaluated as the total energy difference between the singlet- and triplet- states. The molecular electrostatic potential (ESP) was generated using Gaussview 5.0, where red color stands for positive electrostatic potential while the blue stands for negative electrostatic potential.

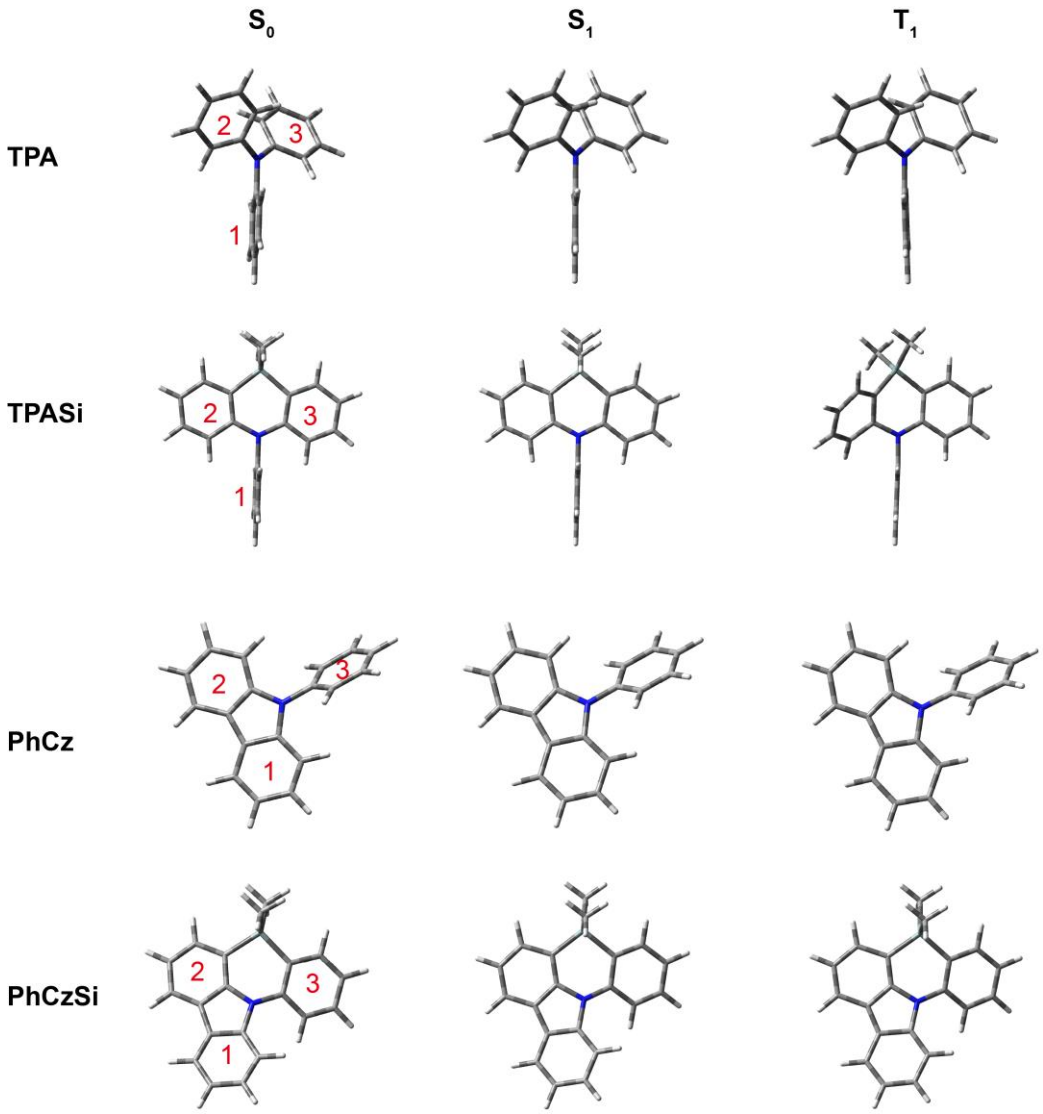

Scheme S3. The optimized molecular geometries of TPA, TPASi, PhCz, and PhCzSi at the ground state (S_0) and the lowest singlet (S_1) and triplet excited states (T_1).

The charge injection and transport and their balance are crucial for optoelectronic compounds; therefore, it is important to investigate their ionization potentials (IPs), electronic affinities (EAs), and reorganization energies (λ) to evaluate the energy barrier for injection and

transport rates of the holes and electrons. The charge (hole and electron) mobility of TPA, TPASi, PhCz and PhCzSi was assessed by using the incoherent hopping model, which assumes a charge transport process between two adjacent reactions $M^{\pm} + M \rightarrow M + M^{\pm}$ where M is the neutral molecule interacting with neighboring oxidized or reduced $M^{\pm}$. The hopping rates of charge transfer can be approximately described by the Marcus–Hush equation:

$$K_{h/e} = \left(\frac{\pi}{\lambda_{h/e} kT}\right)^{1/2} \frac{V_{h/e}^2}{\hbar} \exp\left(-\frac{\lambda_{h/e}}{4kT}\right)$$

where $V_{h/e}$ is the electronic coupling matrix element between neighboring molecules; T is the temperature; k and ħ refer to the Boltzmann and Planck constants, respectively; $\lambda_{h/e}$ is the hole/electron reorganization energy calculated by the following equations[4]:

$$\lambda_h = \lambda_+ + \lambda_1$$

$$\lambda_e = \lambda_- + \lambda_2$$

$$\lambda_+ = E^+(M) - E^+(M^+)$$

$$\lambda_1 = E(M^+) - E(M)$$

$$\lambda_- = E^-(M) - E^-(M^-)$$

$$\lambda_2 = E(M^-) - E(M)$$

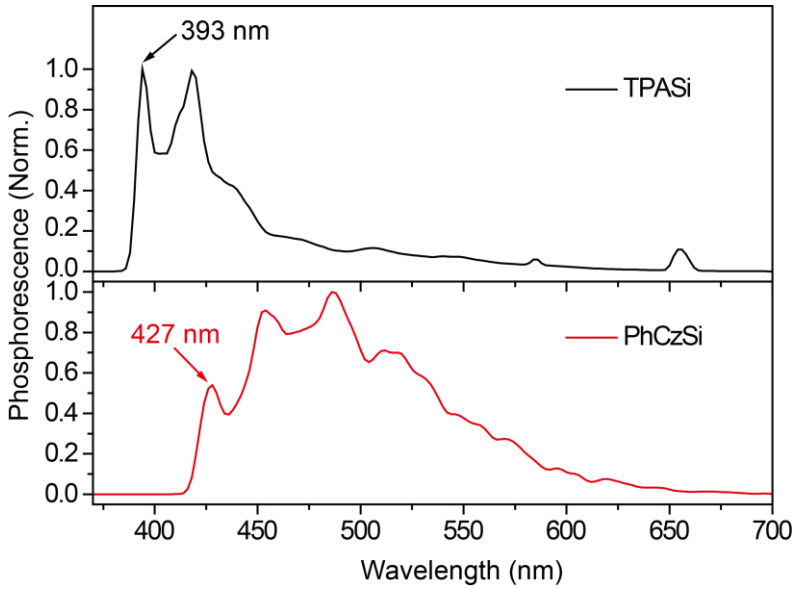

Figure S14. Phosphorescence spectra of TPASi (black) and PhCzSi (red) recorded at 77 K in DCM after a delay of 5 ms.

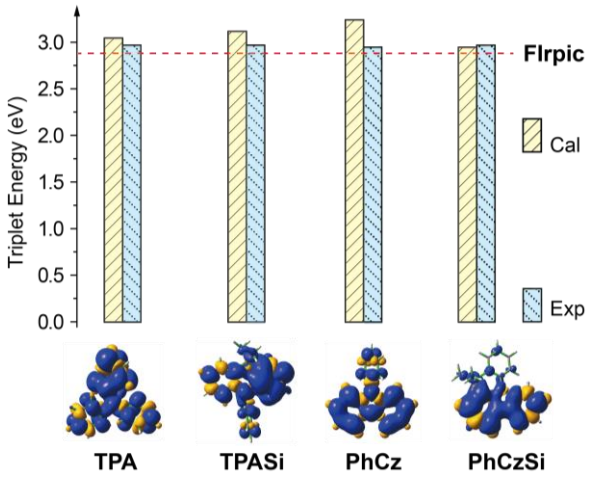

Figure S15. Experimental and theoretical triplet excited state energies and contours of the spin density distributions of the T_1 states of TPA, TPASi, PhCz and PhCzSi.

Table S3. The angles (in º) between the molecular planes of the three phenyl substituents (No. 1, 2, and 3) around N atom from the DFT calculations and single crystals.

Comp.	From DFT calculation									From single crystal		
	S_0			S_1			T_1			S_0		
	(1, 2)	(1, 3)	(2, 3)	(1, 2)	(1, 3)	(2, 3)	(1, 2)	(1, 3)	(2, 3)	(1, 2)	(1, 3)	(2, 3)
TPA	69.92	69.51	69.75	65.80	65.99	66.08	63.72	67.31	62.29	--	--	--
TPASi	89.28	90.72	1.44	85.51	94.58	9.07	71.56	49.78	41.27	85.85	89.38	5.67
PhCz	123.07	123.15	0.04	133.17	133.17	0.29	123.75	123.75	0.18	--	--	--
PhCzSi	8.14	29.83	23.71	10.58	30.49	21.56	10.67	29.74	20.96	10.25	32.89	24.63

Table S4: The ionization potential (IP), electronic affinity (EAs), relaxation energies (λ_+, λ_1, λ_- and λ_2) and reorganization energies (λ_{hole} and $\lambda_{electron}$) of TPA, TPASi, PhCz and PhCzSi (in eV).

Comp.	IP	HEP	EA	EEP	λ_+	λ_1	λ_-	λ_2	λ_{hole}	$\lambda_{electron}$
TPA	6.41	6.30	-1.12	-0.86	0.06	0.06	0.11	0.15	0.11	0.26
TPASi	6.45	6.32	-1.05	-0.76	0.06	0.07	0.16	0.14	0.13	0.29
PhCz	6.84	6.74	-0.87	-0.56	0.05	0.05	0.14	0.16	0.10	0.31
PhCzSi	6.71	6.59	-0.50	-0.24	0.06	0.06	0.13	0.13	0.12	0.26

8. Device fabrication and measurements

The application of phenazasiline derivatives as host materials for blue phosphorescent emitter of Iridium(III) [bis(4,6-difluorophenyl)-pyridinato-N,$C^{2'}$] picolinate (FIrpic) was investigated in a phosphorescent organic light emitting diode (PhOLED). In a general procedure,[5] ITO-coated glass substrate was etched, patterned, and washed with detergent, deionized water, acetone, and ethanol in turn. Organic layers were deposited by high-vacuum ($\approx 4\times 10^{-4}$ Pa) thermal evaporation with a rate of 0.1-0.2 nm s^{-1} at a temperature lower than 80°C. To reduce the ohmic loss, a heavily *p*-doped layer with MoO_x (because of the low doping efficiencies of transition-metal-oxide-based acceptors in amorphous organic matrixes[6]) was directly deposited onto the ITO substrate. The layer thickness and the deposition rate were monitored in situ by an oscillating quartz thickness monitor. The device without encapsulation was measured immediately under ambient atmosphere at room temperature. Electroluminescence (EL) spectra of the devices were measured by a PR655 spectro scan spectrometer. The luminance-voltage and current–voltage characteristics were recorded using an optical power meter and a Keithley 2400 voltage current source. The external quantum efficiency (EQE) of the device was calculated by **Equation 2**.

$$EQE = \frac{\pi e \eta_{cd/A} \int \lambda p(\lambda) d\lambda}{hcK_m \int p(\lambda)\Phi(\lambda) d\lambda} \qquad 2$$

where $\eta_{cd/A}$ is the current efficiency (cd/A); *h* is the Planck constant; c is the speed of light in vacuum; λ is the wavelength (nm); e is the electron charge; p(λ) is the electroluminescent intensity; Φ(λ) is the luminous efficiency; K_m is a constant of 683 lm/W.

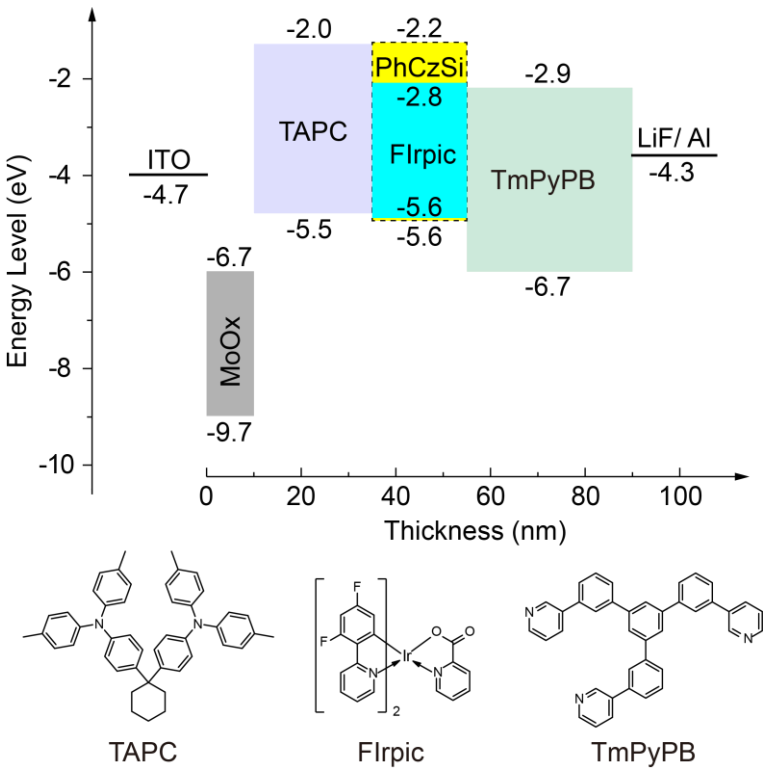

Figure S16. The PhOLED device configuration and energy level diagram using PhCzSi as the host material.

Table S5. The optical and electrochemical properties of the phenazasiline derivatives

Comp.	T_d/T_m (°C)	PLQY[a] %	λ_{abs} (nm) DCM	λ_{abs} (nm) Film	$^{opt}E_g$ (eV)	λ_{em} (nm) DCM	λ_{em} (nm) Film	$^{exp}E_T$ (eV)	CV (eV) HOMO	CV (eV) LUMO	Calculation (eV) HOMO	Calculation (eV) LUMO	$^{cal}E_g$	$^{cal}E_T$
TPA	--	6	301	310	3.64	361	375	3.00	-5.37	-1.72	-4.95	-0.30	4.65	3.03
TPASi	188/110	8	290,312,335	290,325,339	3.60	346	363,429	3.15	-5.43	-1.83	-5.02	-0.43	4.59	3.15
PhCz	--	40	293,328,340	295,328,342	3.57	349,365	388	3.03	-5.68	-2.11	-5.32	-0.65	4.67	3.38
PhCzSi	246/150	37	298,341,354	301,342,356	3.39	370	405,489	2.90	-5.61	-2.22	-5.31	-0.91	4.40	2.88

[a]: Photoluminescence quantum yield (PLQY) in dichloromethane (DCM) at low concentration (1.3×10^{-6} mol L^{-1})

9. References

1. Chun To, S.; Yee Kwong, F. *Chem. Commun*. **2011,** *47*, 5079-5081.

2. Furukawa, S.; Kobayashi, J.; Kawashima, T. *J. Am. Chem. Soc*. **2009,** *131*, 14192-14193.

3. An, Z.; Zheng, C.; Chen, R.; Yin, J.; Xiao, J.; Shi, H.; Tao, Y.; Qian, Y.; Huang, W. *Chem.–Eur. J.* **2012,** *18*, 15655-15661.

4. (a) Yin, J.; Zhang, S.; Chen, R.; Ling, Q.; Huang, W. *Phys. Chem. Chem. Phys*. **2010,** *12*, 15448-15458. (b) Yan, M.; Tao, Y.; Chen, R.; Zheng, C.; An, Z.; Huang, W. *RSC Adv*. **2012**, 2, 7860-7867.

5. Fan, C.; Zhu, L.; Liu, T.; Jiang, B.; Ma, D.; Qin, J.; Yang, C. *Angew. Chem. Int. Ed*. **2014,** *53*, 2147-2151.

6. Han, C.; Zhao, F.; Zhang, Z.; Zhu, L.; Xu, H.; Li, J.; Ma, D.; Yan, P. *Chem. Mater*. **2013,** *25*, 4966-4976.